Tribology International 196 (2024) 109670

Contents lists available at ScienceDirect

Tribology International

journal homepage: www.elsevier.com/locate/triboint

# A machine learning-driven approach to predicting thermo-elasto-hydrodynamic lubrication in journal bearings

Samuel Cartwright [a], Benjamin C. Rothwell [a,*], Grazziela Figueredo [b], Humberto Medina [a], Carol Eastwick [a], James Layton [a], Stephen Ambrose [a]

[a] Mechanical and Aerospace Systems, Faculty of Engineering, University of Nottingham, Nottingham, NG7 2RD, United Kingdom
[b] School of Computer Science, University of Nottingham, Nottingham, NG7 2RD, United Kingdom

ARTICLE INFO

*Keywords:*
Journal bearing
Hydrodynamic lubrication
Machine learning
Neural network
PyTorch
OpenFOAM

ABSTRACT

Traditional methods of evaluating the performance of journal bearings, for example thermal-elastic-hydrodynamic- lubrication theory, are limited to simplified conditions that often fail to accurately model real-world components. Numerical models that include additional phenomena such as cavitation and fully coupled effects like deformation, temperature, pressure and viscosity can be more accurate but require a large amount of computational overhead, making analysis slower and more costly. To address this limitation, a novel machine learning-driven approach is developed to predict the 2D distribution of surface deformation, film thickness, temperature, and pressure across the bearing surface as a function of design variables such as load and speed. The training dataset, generated using a fully coupled Reynolds' Equation solver implemented in OpenFOAM, contains a significantly extended range of conditions than in previous studies with approximately 39 000 000 points encompassing 4925 different test cases. Modelled bearing speeds range from 2000 to 10 000 rpm, while load values are varied between 1 and 30 kN. Predicting surface deformation, film thickness, temperature and pressure across the bearing surface results in a mean absolute percentage error below 0.4 % or better. The work also demonstrates that the trained models have a strong ability to generalise the prediction beyond the original training data range with only a 1 % error at up to 200 % of the highest trained speed. This work also demonstrates that machine learning-based processes are a practical alternative to physics-based numerical modelling, especially in cases where rapid performance evaluation is desired as real-time calculation is possible with significantly reduced computational cost. This has the potential to enable development of rapid design optimisation tools and real-time performance monitoring at high resolution and with low latency. Using consumer hardware, it is found that the neural network-based approach is faster than the existing numerical modelling technique by a factor of over 10 000, enabling real-time predictions of lubrication systems.

## 1. Introduction

Journal bearings are frequently used to support high-speed rotating components due to their unique combination of low friction and wear rates. Despite a long history of applications [1] the design process of such bearings can be slow, as finding an acceptable design requires the optimisation of multiple variables such as the wear rate, power loss, physical dimensions and manufacturing constraints. Evaluation of a prospective design is also difficult as current numerical modelling techniques can be computationally intensive. This is further exacerbated when the expected operating conditions feature particularly high speeds or loads, where more complex coupled physical phenomena including elastic deformation of the components and the effects of heat production in the bearing (such as variation in lubricant viscosity and thermal expansion) must be modelled. As a result of this, there is a clear case for the development of a new modelling process as existing methods are slow and costly for a design environment.

A possible alternative to numerical modelling is the application of Machine Learning (ML). By developing a database of previous results, it can be possible to eliminate the need to solve the same set of coupled Thermo-Elastic Hydrodynamic Lubrication (TEHL) equations repeatedly throughout the design process and by shifting computational overhead away from a recurring cost towards an up-front one, the design evaluation process can be accelerated and greater insights can be gained into the underlying mechanics for further design optimisation.

In general, the effectiveness of ML models depends significantly on the quality of the data used to train them. Previous studies have

* Corresponding author.
*E-mail address:* benjamin.rothwell@nottingham.ac.uk (B.C. Rothwell).

https://doi.org/10.1016/j.triboint.2024.109670
Received 25 September 2023; Received in revised form 19 March 2024; Accepted 14 April 2024
Available online 17 April 2024

investigated the application of ML approaches to model hydrodynamic lubrication problems, however these studies are often limited by insufficient data volume, limited ranges of modelled conditions and low mesh resolutions. This study seeks to address these limitations through the use of higher resolution meshes describing a broader range of speed and load conditions to generate a significantly larger dataset and to demonstrate that ML-based modelling techniques have the potential to enable fast and accurate models applicable for real-world conditions.

One ML technique that has seen widespread adoption in many engineering contexts is the use of feedforward neural networks. They are trained using data from a fully coupled TEHL solver implemented in OpenFOAM [2], and are used to model four important variables for quantifying the performance of a journal bearing: the lubricant film thickness and associated surface deformation, as well as the temperature and pressure distributions across the bearing surface. Feedforward neural networks are chosen to be implemented in this study due to the use of a large, multidimensional dataset. A frequent limitation of Reynolds' Equation-based numerical design tools is that they depend on an initially unknown eccentricity ratio as an input; this is addressed in this study by limiting inputs to known design variables such as the bearing speed and load.

These models are then evaluated against an existing TEHL solver [2] for each modelled variable, and where possible evaluated against experimental data.

## 2. Background

### 2.1. Elastohydrodynamic contact

Modelling of elastohydrodynamic lubrication problems is typically achieved via two different means; solving the Navier Stokes (NS) equations using a discrete approach, or simplifying the NS equations using several assumptions before solving the more problem-specific Reynolds' equation [3] (although other modelling techniques such as molecular dynamics simulation [4] have been demonstrated). An early example of the former approach is by Almqvist (2002) [5]. A low resolution finite-volume mesh is generated for a line-contact EHL problem and solved using commercial computational fluid dynamics (CFD) code. Acceptable solutions are found for cases with smooth geometry, however the author notes that the model requires small under-relaxation factors which significantly slow the convergence of the model in order to avoid problems with numerical instability. Similar results were obtained by Hartinger (2005) [6] who also noted numerical instability under high-load conditions.

One potential benefit of the CFD approach is that the film is considered as a three-dimensional structure, rather than the two dimensions considered by the Reynolds' equation when neglecting through-film variation in pressure and viscosity. Examples of this approach include [6–9]. In isothermal conditions this 2D film approximation is shown to be accurate, however a temperature gradient through the film [10] has been shown to result in viscosity and pressure gradients that limit model performance under high-viscosity conditions [8].

Recent work has allowed some of these limitations to be mitigated by coupling multiple models to better capture the complex physics of EHL conditions [11–13]. Although this is associated with a significantly increased computational cost [14], the modelling of fluid–structure interaction (FSI) under high pressures is found to be more accurate and numerically stable [15]. A greater degree of coupling was developed by Layton (2023) [2] where the film region of an EHL line contact is modelled using the Reynolds' equation technique, while simultaneously coupled to a CFD region to model lubricant flow within a bearing inlet. This approach was found to exhibit high accuracy (with mean errors for pressure and temperature of less than 5% against experimental data [2]) and an average computational time of less than an hour per case. For these reasons, this TEHL model will be used to construct the dataset used in this study.

### 2.2. Machine learning applied to engineering simulation and tribology

The development of ML tools has implications for many fields of engineering, especially those frequently reliant on computational modelling such as fluid mechanics and tribology. A far broader review of recent advances in ML-based tribology than can be practically covered here was published by Paturi (2023) [16].

A multitude of applications of ML for modelling molecular-scale processes have been demonstrated [4,17], where the potential to assist development of new surface technologies or lubricants is significant. The ability to rapidly evaluate ML models using GPU hardware has significant implications for computationally intensive tasks such as CFD - previous work has successfully demonstrated ML models capable of replacing parts of a CFD solver in order to accelerate the solving process. An example of this is the development of a convolutional neural network (CNN) technique for solving the Poisson equation [18]. Accuracy was noted to be inconsistent in some conditions, however this was mitigated using a hybrid approach where the CNN was coupled with a conventional solver. This resulted in a 320% increase in solve speed. Neural network-based models for accelerating simulation of FSI were also documented by Balasubramanian [19] and Güemes [20]. The super-resolution generative adversarial network (SRGAN) documented in [20] is particularly noteworthy here as an additional increase in speed was gained from the model's ability to upscale the mesh used for CFD, enabling faster solve times for the same output resolution by reducing the complexity of the problem. Similar work was published by Kochkov [21] who also noted strong generalisation ability when working with conditions outside of the training data.

Several studies have tested the performance of ML frameworks for predicting the tribological properties of materials. Hasan (2021) tested models for the performance of aluminium alloys using materials and tribological test data [22], noting moderate performance ($R^2$ = 0.83). An unexpected result from this study was that the k-nearest-neighbour algorithm outperformed all of the tested machine learning models (artificial neural networks, support vector machines, random forests and gradient boosted machines). It also observed that model performance was strongly dependent on the distribution of data within the dataset. Slightly improved performance ($R^2$ = 0.91) was obtained for PTFE composite materials by Wang (2023) [23] instead using a gaussian process regression technique. This was followed by a feature importance process to aid in determining the key parameters affecting friction and wear rate of PTFE materials.

Other types of EHL contact have also been modelled using ML processed with similar degrees of success. Issa (2023) [24] trained a model for predicting the minimum film thickness of an EHL point contact with a variety of different aspect ratios. A strong generalisation ability is observed here, but this is attributed to the selection of linearised parameters for training rather than a direct result of the model's predictive power.

### 2.3. Machine learning modelling for journal bearings and other EHL line contacts

Many previous investigations into the use of neural network architectures for journal bearing modelling are limited by a lack of available training data. Early studies such as that by Sinanoğlu [25] utilise an experimental bearing rig from which to derive training data. While real-world data is useful from an accuracy standpoint, it also introduces a constraint by limiting both the number of data points per test, and the number of possible test cases. In this experimental setup, the bearing casing contained 12 pressure tappings around the circumference, limiting the studied area to the bearing centreline. An additional 4 tappings are included in a line along the bearing casing. For each series of tests at a single temperature, this resulted in 48 data points. Multiple feedforward neural networks were trained from these datasets, with each one modelling the 1-dimensional function

relating the angular position $\theta$ to the corresponding pressure value on the centreline. The author noted the close agreement between each model's predictions and the experimental data, however the lack of a divide between training and testing data complicated evaluating the model's ability to generalise. This was further limited by the small scope of each model, as new experimental data is required to train new models in order to consider a new load or speed combination which further increases the cost of developing and deploying such a model.

Further work was published in 2005 [26] with a similar method, investigating the effects of shaft texture rather than lubricant temperature. An identical neural network structure was used, trained on centreline pressure data as previously described. It is stated in the study that one useful application of the neural network approach was that it enabled the interpolation of values between the measured data points [26], however it was not possible to evaluate the accuracy of this method due to the unavailability of unseen testing data. Since the experimental setup and input space were identical to the earlier study [25], the dataset size was equally limited and similar constraints regarding the separation of training and testing data apply.

While these early studies [25,26] are useful as proofs of concept, their real-world applicability is limited due to the use of scaled model bearings. There is a significant difference in the relative load between the scaled model and full-scale components, as the changes in dimensions are relatively small ($l = 70\,\text{mm}$ and $D = 55\,\text{mm}$ [25] vs. $l = 100\,\text{mm}$ and $D = 100\,\text{mm}$ [27]), however the load changes significantly from $8.3\,\text{N}$ to $30\,\text{kN}$. As a result of this, the mean pressure on the scaled bearing is significantly smaller at $2\,\text{kPa}$, in contrast with studies on full-scale bearings [27] where loads up to $30\,\text{kN}$ produce mean pressures of $3000\,\text{kPa}$. The effect of this difference is compounded by the limited speed of $3000\,\text{rpm}$ [25], while other non-scaled studies document behaviour up to $10\,000\,\text{rpm}$ [27]. As the expected pressures are so low, pressure-coupled effects such as elastic surface deformation and heat generation are less significant than under full-scale conditions.

A more recent application was found for optimisation of combustion engine journal bearings [28]. In this case, the previous training data bottleneck was avoided by switching to a Finite Element (FE) model. This enabled a large increase in the volume of data that can be obtained, both by increasing the resolution of an individual test case and by expanding the range of tested conditions. The use of numerical modelling over experimental data avoids a potential problem faced during testing where the presence of pressure tappings in the outer surface interacts with the film, potentially introducing a source of error into the data.

In this newer study [28], 1848 points of data were used compared to 48 in earlier studies [25,26]. Multiple neural networks were trained with the goal of predicting important performance metrics such as the oil loss rate and power loss as a function of the engine speed, oil viscosity and load; these were then used as a cost function for a genetic algorithm, with the goal of optimising for minimum power loss and oil consumption. A Pareto front was established that was deemed to be an improvement in all metrics from the currently established design point. Due to the accuracy of the results from the designed models, this work demonstrated the practicality of the use of feedforward neural networks as design tools in cases where limited experimental data is available.

An alternate approach was documented by Hess [29]. Rather than a complete prediction being obtained from input coordinates or design variables like in earlier studies, this model demonstrated using a CNN to transform an input film thickness field into a predicted pressure field. Strong agreement was observed between the ML approach and the numerical model used to generate training data. One potential drawback of this approach is that it requires knowledge of the rigid film thickness profile before a pressure field can be calculated, although the study does suggest that an iterative approach to varying the eccentricity can allow for a target shaft load to be obtained. It is unclear whether this approach is able to scale for eccentricity values greater than 1, where the idealised shaft and bushing geometries intersect and the rigid film thickness becomes negative in some places.

An example of the potential for ML-based tribology models for performance monitoring is found in Rossopoulos (2021) [30]. A dataset was constructed linking liftoff speed, shaft load and misalignment with models trained to predict each variable as a function of the other two. It is theorised that these models could be paired with onboard sensor data to detect anomalies in the operation of marine journal bearings to aid in the detection and diagnosis of faults earlier than with traditional means.

A Finite Element technique was applied by Kumar et al. [31]. In this case, a similar workflow to [25,26] involved utilising a Hydrodynamic Lubrication solver to generate a dataset by systematically varying the input parameters, which was then employed for training a neural network model. The models trialled displayed good performance when predicting the maximum pressure and minimum film thickness with a maximum error of $\pm 1\%$ [31]. A key limitation of the 2022 study is the mesh size of 36 cells which is reduced down to 2 data points: maximum pressure and minimum film thickness. In addition to this, the finite element model developed for this study does not consider any pressure- or temperature-coupled effects and so the real-world performance under high loads may be impacted.

Several recent studies have identified conditions for obtaining optimum performance of ML models. Baş (2023) [32] noted that performance of an artificial neural network trained on experimental data for predicting friction torque was good for conditions in the hydrodynamic regime, but degraded under boundary or mixed conditions. Gheller (2023) [33] observed that the accuracy of the numerical model was a key factor in the ML model's performance, while Gheller [33] and Marian [34] both found that variation in the model size, dataset size and format all significantly impacted performance. The effect of model size was further documented by Singh (2023) [35], who obtained high accuracy ($R^2 = 0.998$) by maximising the model's parameter count before the onset of overfitting.

This study seeks to expand upon the previous work by significantly increasing the volume of data. More data can be obtained by increasing the resolution of the numerical model's film mesh and by widening the sweep of input parameters that are used to construct the dataset. The physical accuracy of the training data is improved in comparison to existing data-driven models through the use of a fully coupled TEHL model described in Section 3.1. The scope of the models is increased in two ways; firstly, additional variables such as temperature and surface deformation will be predicted in addition to film thickness and pressure. Secondly, the limitation from early studies of predicting centreline values is addressed by designing models capable of predicting the value across the whole bearing surface.

## 3. Materials and methods

### 3.1. TEHL model and numerical procedure for data generation

To construct and train neural network-based models, a training dataset is built describing the bearing's performance across a range of different conditions. This data is generated using a Thermo-Elastic Hydrodynamic Lubrication model implemented in OpenFOAM [2]. This model solves multiple coupled equations to converge on a solution that considers the heat production in the lubricant film, the temperature-dependent viscosity of the lubricant, and the effect of the calculated pressure distribution on the deformation of the shaft and bush. Simulation of cavitation in the low pressure regions is carried out using the Elrod–Adams model [36]. Each section is solved sequentially, and eccentricity ratio is updated iteratively to converge towards a target load.

The highly coupled nature of the system of equations solved by the OpenFOAM model results in slow convergence of the solution due

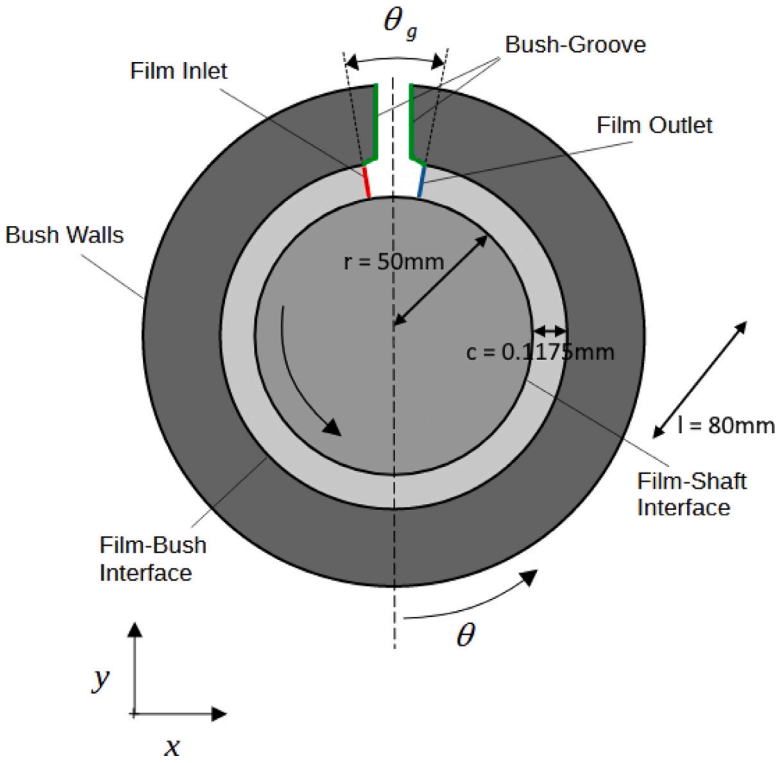


**Fig. 1.** Diagram of the journal bearing geometry used for the TEHL model with relevant dimensions annotated.

to the large number of iterations required. The function for calculating surface deformation is particularly computationally intensive and has the largest effect on computational time, especially as the mesh resolution increases.

The model in OpenFOAM is based on the Reynolds equation [3,37] which is derived based on the thin-film assumptions for hydrodynamic lubrication:

- Pressure gradients normal to the surfaces are negligible.
- The flow is laminar.
- Body forces of the fluid are negligible.
- The fluid is Newtonian.
- Curvature affects are negligible.

Applying these assumptions for a viscous fluid derives the equation:

$$\frac{\partial}{\partial x}\left(\frac{\rho h^3}{12\mu}\frac{\partial P}{\partial x}\right)+\frac{\partial}{\partial z}\left(\frac{\rho h^3}{12\mu}\frac{\partial P}{\partial z}\right)=\frac{\partial}{\partial x}(\rho U h) \tag{1}$$

where p is the pressure, $\rho$ is the density, U is the average velocity between the surfaces, h is the film height, $\mu$ is the dynamic viscosity and $x$ and z are special dimensions in the circumferential and axial directions respectfully. Cavitation affects in the fluid are modelled using the Elrod–Adams algorithm [36] which incorporates a pressure–density function and switch variable:

$$\Theta=\frac{\rho}{\rho_{cav}} \tag{2}$$

$$P=P_{cav}+g\beta\ln(\Theta) \tag{3}$$

$$\frac{\partial}{\partial x}\left(\frac{g\beta h^3}{12\mu}\frac{\partial\Theta}{\partial x}\right)+\frac{\partial}{\partial z}\left(\frac{g\beta h^3}{12\mu}\frac{\partial\Theta}{\partial z}\right)=U\frac{\partial\Theta h}{\partial x'} \tag{4}$$

where g is the switch variable, $\beta$ is the bulk modulus of the fluid and $\Theta$ is the relative density. The switch variable is dependent on $\Theta$ and solved using an iterative procedure:

$$\begin{aligned}&\Theta<1, \quad g(\theta)=0\\&\Theta\geq 1, \quad g(\theta)=1\end{aligned} \tag{5}$$

Elastic deformation of the surfaces from the pressure field in the fluid is estimated using the half-space approximation:

$$\begin{aligned}h_d(x,z)&=\frac{2\pi}{E'}\iint\frac{P(x_i,z_k)}{\sqrt{(x-x_i)^2+(z-z_k)^2}}dx_i dz_k\\E'&=\frac{2}{\frac{1-v_1^2}{E_1}+\frac{1-v_2^2}{E_2}}\end{aligned} \tag{6}$$

where E′ is the effective Young's modulus. An energy equation is included to approximate the temperature in the fluid:

$$\frac{\partial}{\partial x}\left(c_p\rho uT\right)+\frac{\partial}{\partial z}\left(c_p\rho wT\right)-k\frac{\partial^2 T}{\partial y^2}=\mu\left(\frac{\partial u}{\partial y}^2+\frac{\partial w}{\partial y}^2\right) \tag{7}$$

where u and w are velocity components in the $x$ and z directions respectively, $c_p$ is the specific heat capacity, $\bar{h}$ is the relative film height ($\frac{h}{C}$), k is the thermal conductivity and $U_s$ is the shaft surface velocity. A temperature–viscosity model is also incorporated:

$$\mu_T=\mu_0 e^{\gamma_T(T-T_{ref})} \tag{8}$$

where $\gamma$ is the temperature–viscosity coefficient and $\mu_0$ is the viscosity at temperature $T_0$.

Temperature in the adjacent bush region modelled with a conduction equation:

$$k\left(\frac{\delta T}{\delta x}+\frac{\delta T}{\delta y}+\frac{\delta T}{\delta z}\right)=0 \tag{9}$$

The solution procedure is outlined in Fig. 2. An iterative procedure is applied for the TEHL system of equations. An outer iterative procedure is applied between the TEHL and solid bush regions to converge towards a coupled solution.

### 3.2. Training dataset generation

The bearing dimensions and other parameters are given in Table 1. The dimensions are chosen to match the setup documented by Bouyer & Fillon [38] (illustrated in Fig. 1), to ease the process of evaluating

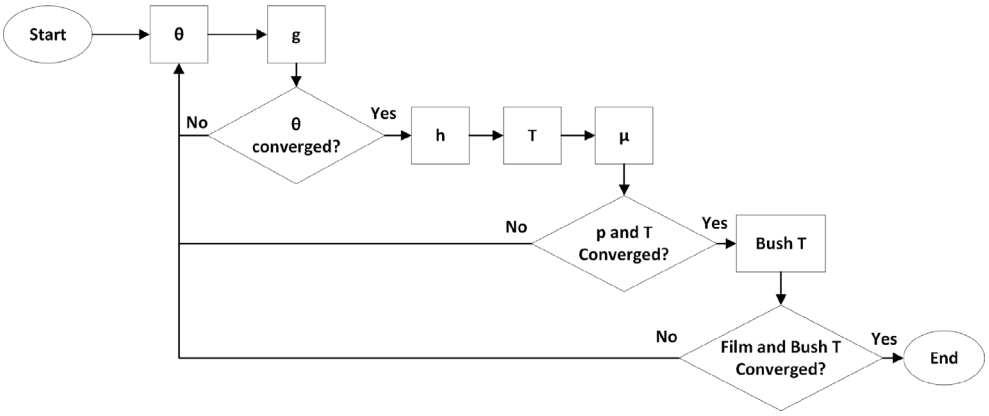


**Fig. 2.** Flowchart of the OpenFOAM model iterative process.

**Table 1**
A table of the input variables and constants for the TEHL model.

| | | |
|---|---|---|
| Bearing length (mm) | l | 80 |
| Bearing diameter (mm) | d | 100 |
| Clearance (μm) | c | 117.5 |
| Lubricant viscosity (Pa s, 40 °C) | $\mu$ | 0.0277 |
| Young's modulus (GPa, shaft) | $E_s$ | 90 |
| Young's modulus (GPa, bush) | $E_b$ | 90 |

against experimental data. The mesh dimensions for the OpenFOAM model were selected according to the mesh study conducted in [2], such that further refining the mesh results in a <1% change in the predicted temperature values.

The training dataset for this model is constructed by conducting a parametric sweep, varying both the speed and load. The speed ranges from 2000 to 10 000 rpm in 500 rpm increments, while the load is varied from 1 to 30 kN in 100 N steps. 30 test cases are selected with speeds of 2250, 3750, 5250, 6750, 8250 and 9750 rpm, and loads of 5, 10, 15, 20 and 25 kN. These are chosen so that the behaviour of the model is well documented under a variety of load conditions, while the intermediate spacing of the speed values ensures that the model is not tested on data that it was already exposed to during training. The distribution of training and testing data is illustrated in Fig. 3.

For each load–speed combination in the dataset, the OpenFOAM model is solved and the film mesh is extracted, for a total of 4925 training cases and 30 test cases. These are compiled into a training and testing dataset where each line in the dataset represents a single mesh cell, containing the cell's co-ordinates and the film thickness, deformation, temperature and pressure at that location. Due to the assumption of no shaft misalignment, it is known that all of the aforementioned modelled outputs are symmetrical across the bearing midplane (located at $\frac{z}{l} = 0.5$). Due to this, the full mesh can always be reconstructed by taking one half and mirroring across the midplane. By altering the prediction process to only model half of the surface and then reflecting the result, only 8000 cells of each 16 000 cell mesh are needed. As a result, the dataset size can be reduced by 50% with no loss in information, to speed up the training process. The final training dataset size is 39 416 000 points (7.8 GB), and evaluation is performed on 240 000 unseen points.

Each case has a mean convergence time of 584 s. By running multiple instances of the solver in parallel, the dataset can be generated more efficiently; using 96 CPU cores, generation of the training data took 10 h. The full dataset is then preprocessed and split into training, validation and testing datasets as illustrated in Fig. 4.

### 3.3. Data preprocessing

As a result of their generation by the parametric sweep outlined in Section 3.2, all of the input variables have a uniform distribution in the

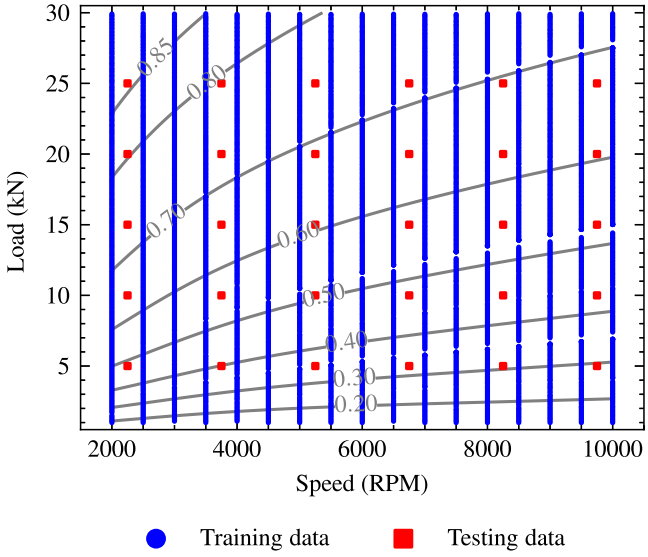


**Fig. 3.** Distribution of training and testing data. Contours of constant $\epsilon$ are plotted. It can be seen that gaps are present for some eccentricity values; this is due to the OpenFOAM model deviating from the target load under some specific conditions. 5 combinations are missing from an expected total of 4930.

**Table 2**
New preprocessing algorithms for the deformation and pressure categories.

| | |
|---|---|
| Deformation | Calculate $log_{10}$ of each value, then rescale into the range (0,1). |
| Pressure | Shift all values up by the minimum value + 1 atm to eliminate negative values, then calculate $log_{10}$ of each variable. Finally, standardise the dataset to have a mean of 0 and standard deviation of 1. |

training data. As such, preprocessing these variables by linear rescaling into the range (0, 1) is appropriate [39]. However, the output variables (film thickness, deformation, temperature and pressure) follow more complex distributions as shown in Fig. 5.

It can be seen that the film thickness and temperature columns are approximately symmetrical with little skew and few outliers, so these perform well when preprocessed by linear rescaling similar to the inputs. For the deformation and pressure columns, there are a large number of outliers corresponding to the maximum values and a significant overrepresentation of the minimums. This is addressed using a new preprocessing scheme defined in Table 2.

The results of applying this new preprocessing scheme are shown in Fig. 6. This technique works well for the deformation distribution, as the skewness is significantly reduced and there are no longer any

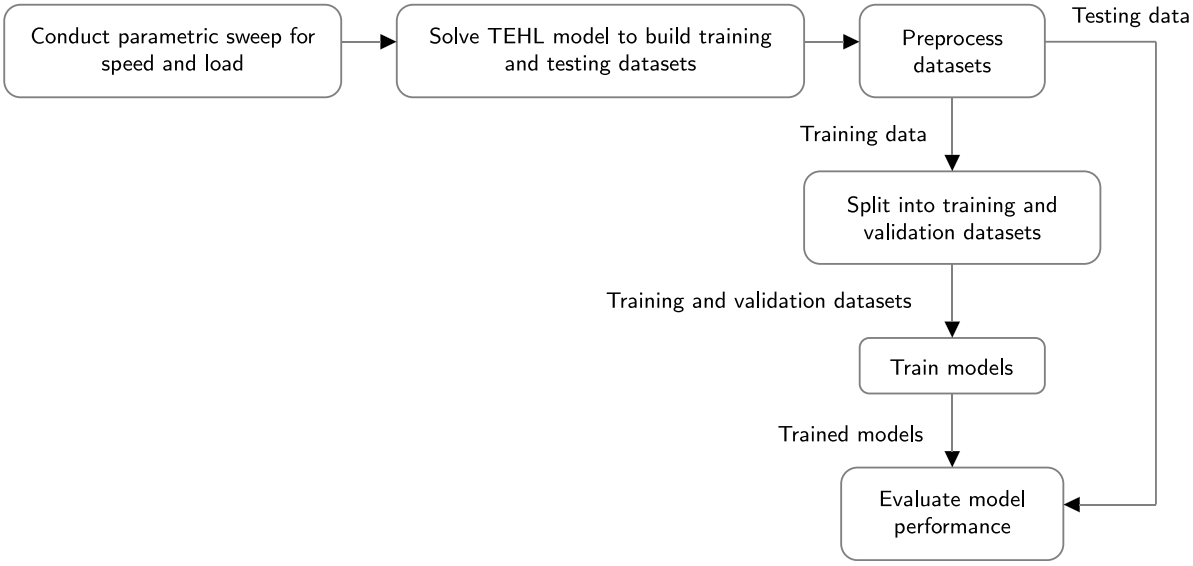


**Fig. 4.** Diagram showing the data flow for generating the training dataset and using it to train the neural network models.

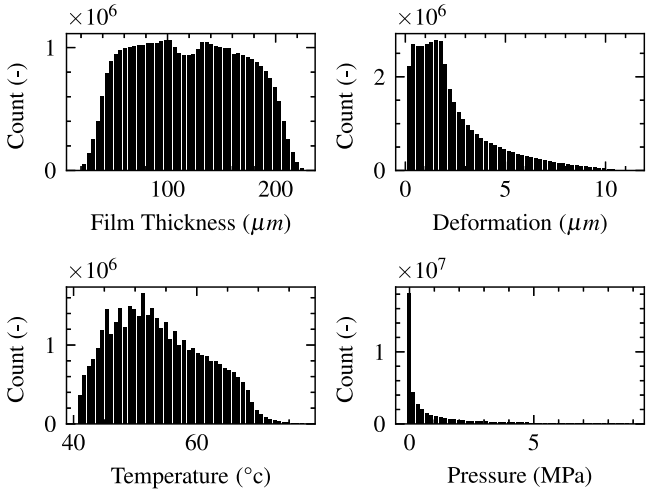


**Fig. 5.** Histograms of the distribution of the four output variables within the training dataset, with no preprocessing applied.

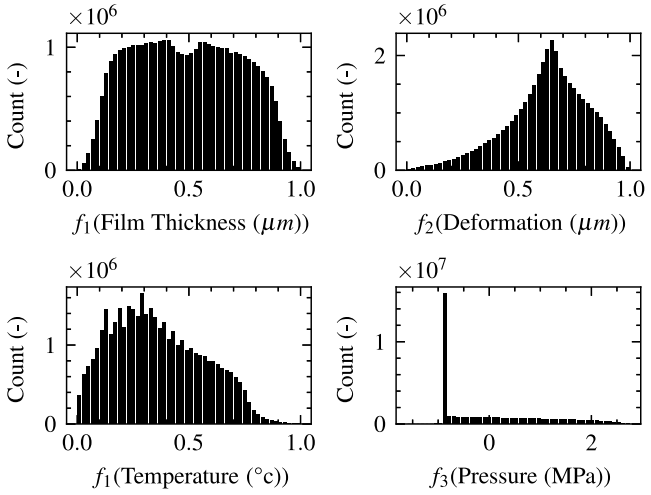


**Fig. 6.** Distributions of the output variables in the training dataset after applying the preprocessing algorithms.

significant outliers. The algorithm could be further fine-tuned to obtain a symmetrical distribution by altering the base of the logarithm function applied to the data. The technique for the pressure column is also an improvement as for the pressures above ambient the distribution is approximately uniform, however it can still be seen that low pressures (resulting from the majority of every mesh in the test data containing many cells at ambient pressure) is significantly overrepresented. Thus, some further refinement to this algorithm could improve the performance of the pressure-predicting neural network model.

### 3.4. Neural network model structure

#### 3.4.1. Potential neural network model architectures

Several different neural network structures have been proposed during earlier studies. For example, Sinanoğlu (2004) [25] and (2005) [26] demonstrated predicting centreline pressure by constructing a neural network to model pressure as a function of the angular position $\theta$, but requiring multiple different neural networks to model different load and speed conditions.

Kumar et al. [31] demonstrated using loads and speeds as inputs to predict minimum and maximum values of the film thickness and pressure respectively. This method could be expanded on to predict the whole distribution of each variable across the bearing surface by adding multiple new pressure and film thickness outputs representing different co-ordinates, however there are several drawbacks to this approach. Firstly, the resolution of the output distribution is fixed as it is determined by the ML architecture itself. This can make evaluation of the model more difficult by requiring interpolation if the experimental or numerical data it is evaluated against does not align with the neural network's output coordinates. Additionally, this approach would require a very large number of network parameters, increasing further if additional variables such as deformation and temperature are also desired as outputs.

One solution to this is to combine the two ML architectures, from Kumar [31] and Sinanoğlu [25], to create a model that accepts as inputs both the load conditions and coordinate (adding an extra coordinate for axial position $z$ to enable modelling of values across the two dimensional bearing surface) and outputs the relevant variables such as film thickness, deformation, temperature and pressure. This approach

avoids the fixed-resolution problem as the locations to evaluate the model are determined by the user, resulting in a built-in interpolation function. Trials were ran using this architecture, however the model failed to converge during training as it was unable to simultaneously learn the multiple different functions that describes each of the outputs as a function of both the load and the location on the bearing surface. This could potentially be alleviated by expanding the size and depth of the neural network, however the cost of this is an increased computational overhead resulting in slower training and evaluation.

An alternative solution, rather than creating a single unified model, is to design multiple smaller independent models, each one focusing on modelling a single output variable as a function of both the load conditions and the coordinate. This combines the advantages of both approaches:

- The parameter count is minimised for faster training and evaluation.
- There is no fixed resolution and interpolation across the input coordinate space occurs implicitly.
- The models can be evaluated at any given location without needing to model the entire surface and extract a specific point afterwards.
- The independent nature of having multiple models means that new variables can be modelled without needing to redesign and retrain the existing neural networks.
- The hyperparameters for each separate neural network can be separately optimised for the best performance.

#### 3.4.2. Final neural network model structure

For the reasons outlined in Section 3.4.1, the chosen model format consists of four independent neural networks, each one designed to predict one of the output variables as a function of the load, speed, axial position $z$ and angular position $\theta$. The neural network's hyperparameters were determined via experimentation; the final design features 8 hidden layers of 48 neurons each, for each model. The ReLU activation was tested, however with the chosen preprocessing scheme regularly producing negative inputs, this function resulted in training instability. The Sigmoid function was instead selected due to its symmetry with positive and negative values.

Lower dimensional models with fewer layers were found to perform worse with larger outlier errors. Increasing the model complexity was found to improve performance, without raising the risk of overfitting due to the dataset being significantly larger than the parameter count of the model. Despite this, a smaller model with 4 hidden layers of 24 neurons was found to display marginally better performance outside of the training data (documented in Section 4.5). A comparison between the models with 4 hidden layers of 24 neurons, and 8 hidden layers of 48 neurons, is shown in Fig. 7 where increasing the model complexity reduces the mean percentage error by 0.6%. Further work could expand on this by conducting multiple independent hyperparameter optimisation processes on each of the different neural network models.

### 3.5. Neural network model training

Each model was trained using an Nvidia Tesla V100 GPU. Training times were different for each model, with the loss calculated per model ceasing to improve after 380 to 760 epochs. With each epoch taking an average of 377 s, this results in a training time of between 40 and 80 h. The training hyperparameters are listed in Table 3.

### 3.6. Evaluation process

The models are to be evaluated by comparing the resulting predictions both to the OpenFOAM model and to experimental data. To compare against the OpenFOAM model, the full distribution of each variable across the bearing surface is predicted for each of the test cases defined in Fig. 3, to ensure that the behaviour of the model under a wide range of possible inputs is documented. The model will be evaluated at the same resolution as the resulting mesh from the OpenFOAM model, so that cell-wise errors can easily be calculated by subtracting one array from the other.

After calculating the full set of testing data, it can be filtered in several ways to analyse the performance of the model. Thus, the relative error is calculated for:

- The entire bearing surface for every test case, to capture the performance across all of the input variables.
- The centreline in each test case, to enable comparison against experimental data which frequently focuses on measuring pressure and film thickness variation along the centreline.
- The minimum and maximum value for each variable in each test case.

Additionally, the times to evaluate each model are compared to validate the ML-based approach's applicability for rapid or real-time modelling of bearing performance.

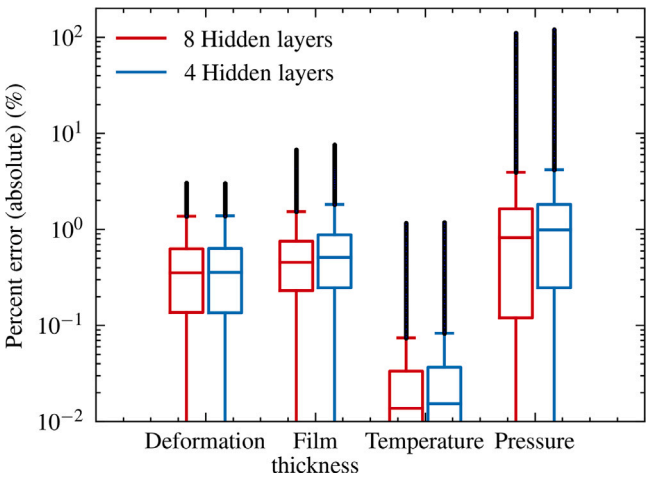


**Fig. 7.** Comparison of neural network models with 4 and 8 hidden layers with 24 and 48 neurons in each layer respectively.

**Table 3**
Hyperparameters for training each of the neural network models.

| | |
|---|---|
| Optimiser | Adagrad [40] |
| Loss function | L1 loss (Mean absolute error) |
| Batch size | 512 |
| Learning rate | 0.03 |
| Learning rate scheduling | 0.5% decay every 10 epochs |

## 4. Results and discussion

### 4.1. Comparison of evaluation time

A significant reduction in evaluation time is observed with the ML-based model, documented in Table 4. The time taken is reduced by 99.990%, a reduction by a factor of 10 300. The neural networks were evaluated using an AMD Ryzen 5 3600 CPU; it is expected that even faster performance could be obtained using more specialised hardware such as CUDA-supporting GPUs [41] as significant increases in speed are documented when evaluating neural networks using GPUs [42] especially as the batch size increases.

The total computational capacity expended to produce the training dataset and train a model is approximately 1440 core-hours. The reduction in computational work resulting from evaluating one of the neural network models instead of the numerical OpenFOAM model is

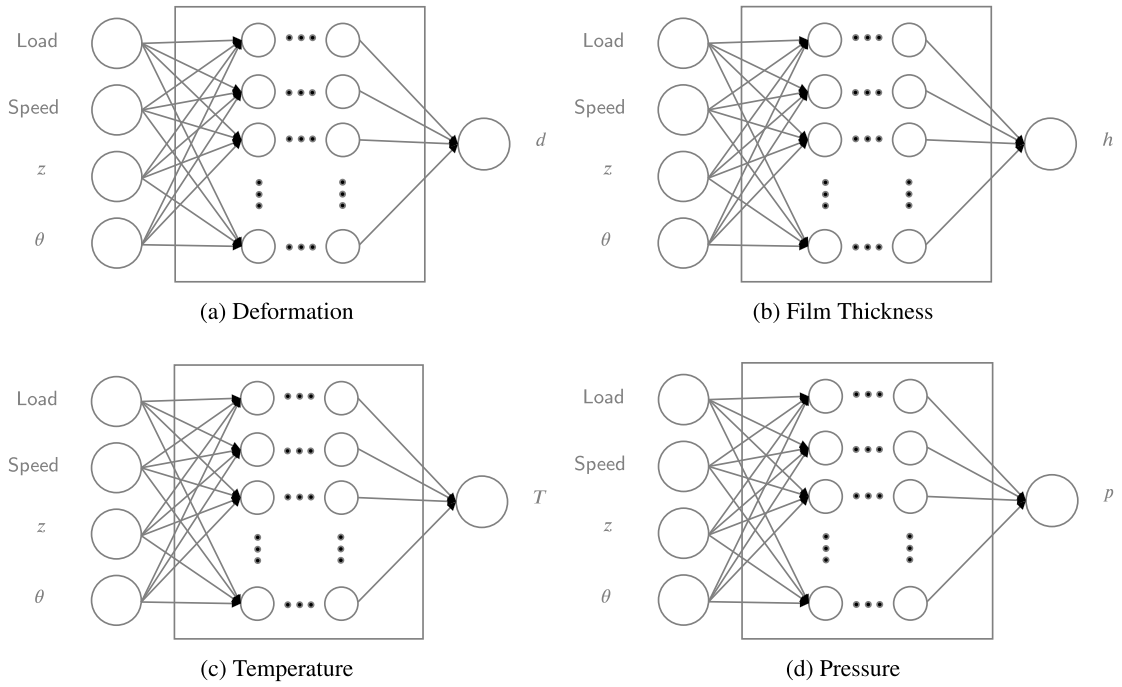


**Fig. 8.** Diagrams of the final model structures for predicting each output variable (deformation, film thickness, temperature and pressure).

**Table 4**
A comparison of the mean evaluation time of the OpenFOAM model against the time to evaluate all four models shown in Fig. 8. The usefulness of lubrication models that can be evaluated at high speed is reviewed by Paturi et al. [16].

| Model | Mean evaluation time (s) |
|---|---|
| OpenFOAM | 584 |
| 4× Neural networks | 0.0567 |

**Table 5**
Summary of the magnitude of the percentage errors when predicting the state of the whole bearing surface.

| Variable | Mean error (%) |
|---|---|
| Film thickness | 0.086 |
| Surface deformation | 0.20 |
| Temperature | 0.0036 |
| Pressure | 0.39 |

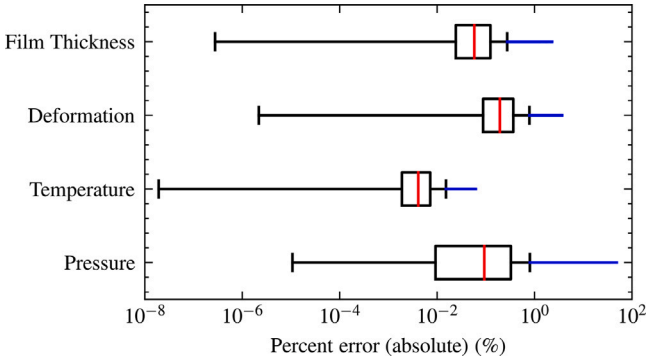


**Fig. 9.** Diagram of the distribution of percentage errors for each variable when predicting the entire bearing surface for every test case.

0.16 core-hours. As a result, the expected break-even point for energy expenditure is reached after evaluating the neural network models around 8900 times.

Due to the ability to greatly parallelise the process of constructing these neural networks, especially when generating training data, much of the computational work to generate these models occurs concurrently. The total time for generating the training dataset and training the models was around 70 h. The time saved by evaluating the neural networks rather than the OpenFOAM model is, on average, 583.45 s. Thus, the break-even point for time occurs much sooner, after using the neural networks 430 times.

### *4.2. Whole-mesh prediction of film thickness, temperature, pressure and surface deformation*

Across the whole 240 000-point testing dataset, the mean absolute percentage errors are shown in Table 5. All variables have a mean error of less than 0.4%.

Additionally, the complete distribution of mean absolute percentage errors for the whole testing dataset is illustrated in Fig. 9.

It can be seen that the majority of errors for all variables are below 1%, however there are a large number of outliers especially for the deformation and pressure variables. This is partially a result of plotting data spanning many orders of magnitude in this format (pressure errors in this dataset vary from $10^{-5}$% to 49%) however there is a notable trend of the relative error increasing for small pressure values, as shown in Fig. 11(a). The large-scale structure of the dataset, visualised by the whole-surface predictions for a set of inputs with intermediate load and speed values from the test dataset in Fig. 10, is in close agreement. It can be seen that far more deviation from the numerical model occurs for small values of pressure than for large ones. As this effect does not occur as significantly for the deformation values in Fig. 11(b), it is likely this results from the poor performance of the pressure preprocessing algorithm documented in Section 3.3.

### *4.3. Prediction of centreline pressure profiles*

When limiting the scope of the analysis to the bearing centreline, the trend of decreasing errors at larger pressure values becomes more

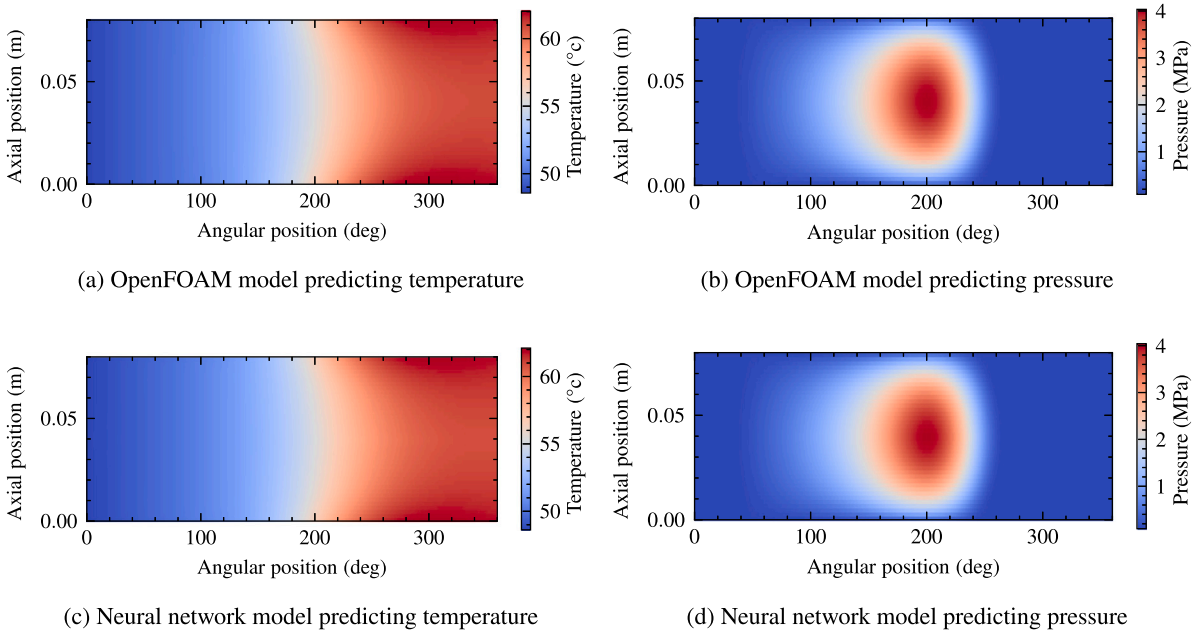


**Fig. 10.** A comparison of the predicted temperature and pressure fields from the OpenFOAM and neural network models, at 6750 rpm and 15 kN.

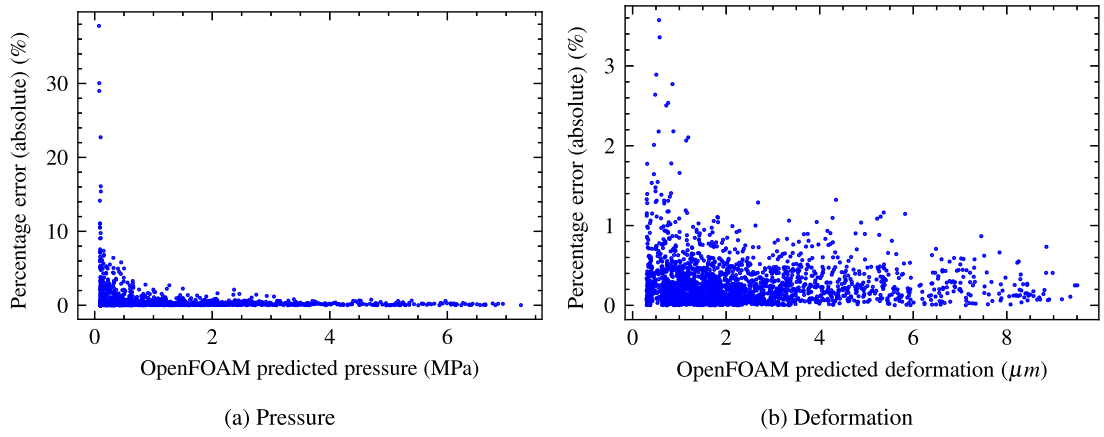


**Fig. 11.** Scatter plots comparing the magnitude of the variable to the percentage error for each point in the test dataset.

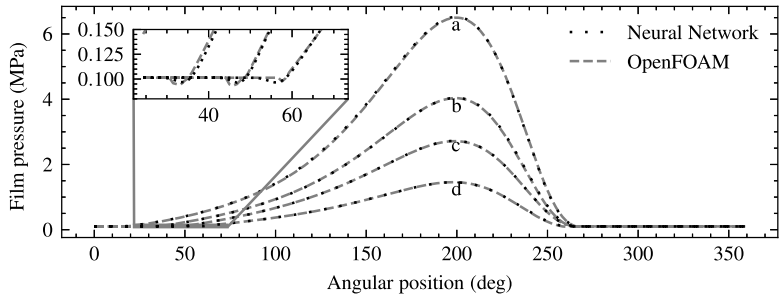


**Fig. 12.** A comparison of the OpenFOAM and neural network models when predicting centreline pressure at four unseen conditions: (a) 9750 rpm, 25 kN (b) 6750 rpm, 15 kN (c) 5250 rpm, 10 kN (d) 2250 rpm, 5 kN.

visible. Fig. 12 shows a comparison of the centreline pressure as predicted by the OpenFOAM and neural network models. It can be seen that for all of the values above the ambient pressure, the agreement between the two models is extremely high. The areas responsible for the greater percentage errors are also visible around $\theta = 40$ to 60 deg, where the small difference in the shape of the curve as the pressure begins to rise produces percentage differences of up to 50%.

### 4.4. Prediction of minimum and maximum points

The minimum and maximum values for each variable are not calculated directly; instead, they are derived by predicting the full distribution and searching the resulting 2D array for the largest or smallest value. For the deformation, temperature and pressure the maximum value is taken, while the minimum is used for film thickness. When

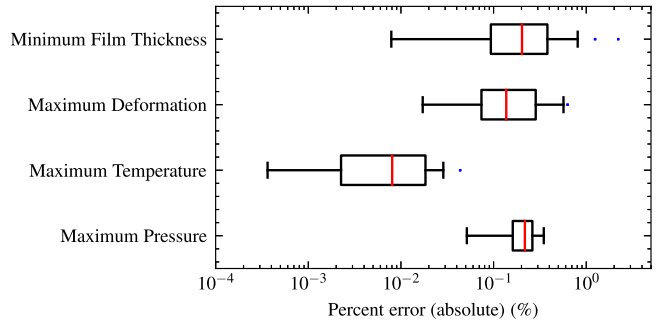


**Fig. 13.** Diagram of the distribution of percentage errors for each variable when predicting the minimum or maximum values.

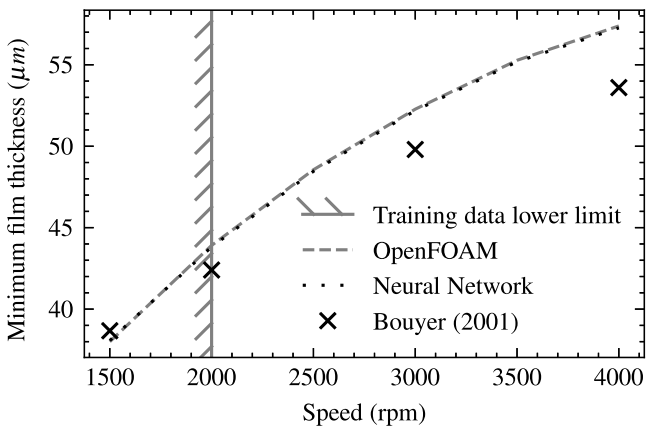


**Fig. 14.** A plot of minimum film thickness vs. speed for a 9 kN load. The lower limit of the speed data contained in the training dataset (2000 rpm) is overlaid.

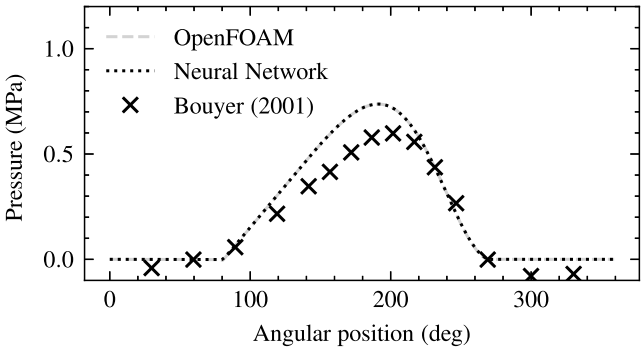


**Fig. 15.** A plot of centreline pressure vs. angular position for a speed of 4000 rpm and a load of 3 kN.

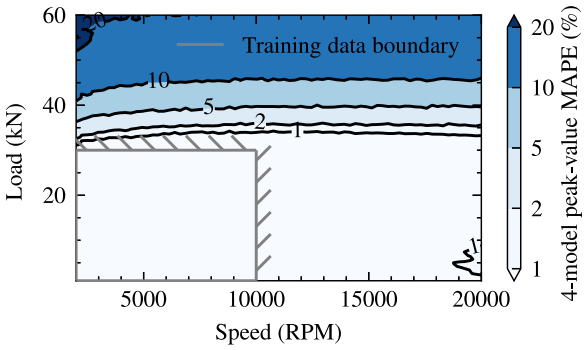


**Fig. 16.** A plot showing average percentage error in minimum film thickness, maximum temperature, maximum pressure and maximum deformation for test cases outside of the training data.

limited to the minimum and maximum values, the mean accuracy across all of the conditions is better for deformation and pressure, but slightly worse for film thickness and temperature.

All errors are within ±0.8% with the exception of two outliers when predicting the minimum film thickness, with errors of −1.2 and -2.2%. These occurred at (3750 rpm, 25 kN) and (2250 rpm, 25 kN) respectively, which are the two smallest film thickness values in the test dataset (see Fig. 13).

### 4.5. Evaluation against experimental data

Both the neural network models and the OpenFOAM model are compared against the experimental data in Bouyer (2001) [38]. Two categories are identified to compare the performance of the two types of model:

- Minimum film thickness as a function of speed, under a 9 kN load.
- Pressure on the centreline as a function of the angular position with a speed of 4000 rpm and a load of 3 kN.

In Fig. 14, it can be seen that both the neural network and OpenFOAM model overestimate the film thickness for the majority of cases, although this trend does not hold for the lowest speed case. One notable observation here is that the neural network and OpenFOAM model are in close agreement at all points, even at the 1500 rpm point. This is evidence of the neural network model's ability to generalise and successfully extrapolate, as the training data contains no information for any speeds lower than 2000 rpm. Performance of the model outside of the training data is further demonstrated in Fig. 16. For each test case, the minimum film thickness and maximum pressure, temperature and deformation are calculated. A percentage error is determined for each, and a single value is obtained by calculating the mean of the four errors.

It can be seen in Fig. 16 that the peak value Mean Absolute Percentage Error (MAPE) for the four output variables remains below 1% for almost all speed inputs up to 20 000 rpm. However, when increasing the load beyond the limit of the training data 30 kN the error quickly increases, although only a small fraction of test points at a maximum load of 60 kN and minimum speed of 2000 rpm exceed an average error of 20%. This region comprises of test cases with eccentricity values between 1.0 and 1.02, while the highest value found in the training data is 0.8.

The errors measured on test cases outside of the training dataset are approximately independent of speed, but increase significantly with load. This is expected given results from experimental work, in which eccentricity approaches a constant as speed increases [43] and pressure has significantly smaller variation due to speed than to load [38], resulting in smaller changes in the output with respect to speed than to load. The strong extrapolation performance is consistent with findings from related studies such as Hess (2021) [29] and Kumar et al. (2022) [31].

Fig. 15 plots the predicted centreline pressure against experimental data. As with Fig. 14, the agreement between the neural network and OpenFOAM models is good, however in this test they both perform worse when compared against the experimental data.

It can be seen that in both tests, the neural network models are able to match the predictions of the OpenFOAM model with a high degree of accuracy; the deviation of the neural networks from experimental data is therefore primarily a result of the inaccuracy of the numerical model itself, rather than a consequence of the neural networks failing to adequately learn the required function. However, the neural network-based approach is essentially model-independent - it is expected that

the neural networks could be trained similarly well for any other numerical model, and therefore the real-world accuracy of this method would increase at a rate similar to the most accurate numerical model available.

## 5. Conclusions

In this study it is established that the multi-model neural network approach is able to closely match the performance of existing numerical modelling techniques once a dataset is constructed and a model is trained, with a reduction in mean solution time of 99.990% while introducing a mean error of less than 0.4%. This reduction in solution time allows for accurate real-time predictions to be made, enabling rapid design evaluation for design optimisation [16,35], as well as for real-time monitoring of the bearing performance during operation. Current experimental setups frequently require invasive sensing techniques such as pressure tappings through the surface of the bush [25,26,38], which have the potential to disrupt the formation of the lubricant film in the high pressure region and affect the load capacity of the bearing. One possible solution to this would be to obtain measurements from regions of the bearing which are less sensitive to alterations to the bearing surface; these measurements could then be coupled with a neural network-based digital twin model to estimate the conditions elsewhere in the bearing where they are difficult to directly measure. Monitoring performance this way using numerical models results in an extremely low temporal resolution and high latency due to the comparatively long convergence time of the model. This approach could potentially extend the service lives of journal bearings in operation by improving the ability to detect the anomalous conditions that indicate the necessity of servicing or replacing components.

One key limitation of the model presented in this work is that the dimensions of the bearing in this model are fixed, alongside other physical quantities such as the lubricant viscosity at the reference temperature, the shaft and bush material properties and the shaft misalignment angle. While this is not a problem for the performance monitoring application, the usability of the model could be expanded by adding additional inputs for these variables to build a more general model, taking full advantage of the ability to model each value in two dimensions and enabling the bearing design to be optimised for minimal heat generation (or any other metric).

## CRediT authorship contribution statement

**Samuel Cartwright:** Writing – review & editing, Writing – original draft, Visualization, Validation, Software, Resources, Methodology, Investigation, Formal analysis, Data curation, Conceptualization. **Benjamin C. Rothwell:** Writing – review & editing, Writing – original draft, Supervision, Project administration, Funding acquisition, Conceptualization. **Grazziela Figueredo:** Writing – review & editing, Writing – original draft, Supervision, Project administration, Methodology, Investigation. **Humberto Medina:** Supervision, Writing – review & editing. **Carol Eastwick:** Supervision, Project administration, Funding acquisition, Writing – original draft, Writing – review & editing. **James Layton:** Software, Writing – original draft, Writing – review & editing. **Stephen Ambrose:** Conceptualization, Software, Writing – original draft, Writing – review & editing.

## Declaration of competing interest

The authors declare that they have no known competing financial interests or personal relationships that could have appeared to influence the work reported in this paper.

## Data availability

The data that has been used is confidential.

## Acknowledgements

The authors thank Rolls-Royce plc and the EPSRC for the support under the Prosperity Partnership Grant Cornerstone: Mechanical Engineering Science to Enable Aero Propulsion Futures, Grant Ref: EP/R004951/1.

## References

[1] Dowson D. History of tribology. second ed.. Wiley; 1998.
[2] Layton J, Rothwell BC, Ambrose S, Eastwick C, Medina H, Rebelo N. A new thermal elasto-hydrodynamic lubrication solver implementation in OpenFOAM. Lubricants 2023;11(7):308.
[3] Dowson D, Higginson GR. A numerical solution to the elasto-hydrodynamic problem. J Mech Eng Sci 1959;1(1):6–15. http://dx.doi.org/10.1243/jmes_jour_1959_001_004_02.
[4] Ewen JP, Spikes HA, Dini D. Contributions of molecular dynamics simulations to elastohydrodynamic lubrication. Tribol Lett 2021;69(1):24. http://dx.doi.org/10.1007/s11249-021-01399-w.
[5] Almqvist T, Larsson R. The Navier–Stokes approach for thermal EHL line contact solutions. Tribol Int 2002;35(3):163–70. http://dx.doi.org/10.1016/S0301-679X(01)00112-8.
[6] Hartinger M, Gosman D, Ioannides S, Spikes HA. CFD modelling of elastohydrodynamic lubrication. In: World tribology congress III. Vol. World Tribology Congress III, Volume 1, 2005, p. 531–2. http://dx.doi.org/10.1115/wtc2005-63840.
[7] Hartinger M, Gosman D, Ioannides S, Spikes H, Asme. Thermal effects in an elastohydrodynamic line contact using a CFD approach. In: ASME/sTLE international joint tribology conference. 2008, p. 179–80, URL: <GotoISI>://WOS:000254339300047, Hartinger, Markus Gosman, David Ioannides, Stathis Spikes, Hugh he, liu/V-6567-2019 Spikes, Hugh/0000-0001-7250-8995.
[8] Hartinger M, Dumont ML, Ioannides S, Gosman D, Spikes H. CFD modeling of a thermal and shear-thinning elastohydrodynamic line contact. J Tribol-Trans ASME 2008;130(4). http://dx.doi.org/10.1115/1.2958077.
[9] Hartinger M, Reddyhoff T. CFD modeling compared to temperature and friction measurements of an EHL line contact. Tribol Int 2018;126:144–52. http://dx.doi.org/10.1016/j.triboint.2018.05.012.
[10] Bruyere V, Fillot N, Morales-Espejel GE, Vergne P. Computational fluid dynamics and full elasticity model for sliding line thermal elastohydrodynamic contacts. Tribol Int 2012;46(1):3–13. http://dx.doi.org/10.1016/j.triboint.2011.04.013.
[11] Hajishafiee A, Dini D, Zaki T, Kadiric A, Ioannides S. Modelling elasto-hydrodynamic lubrication using CFD. 2012.
[12] Hajishafiee A, Kadiric A, Ioannides S, Dini D. A coupled finite-volume CFD solver for two-dimensional elasto-hydrodynamic lubrication problems with particular application to rolling element bearings. Tribol Int 2017;109:258–73. http://dx.doi.org/10.1016/j.triboint.2016.12.046.
[13] Dhande DY, Pande DW. Multiphase flow analysis of hydrodynamic journal bearing using CFD coupled fluid structure interaction considering cavitation. J King Saud Univ, Eng Sci 2018;30(4):345–54. http://dx.doi.org/10.1016/j.jksues.2016.09.001.
[14] Almqvist T, Larsson R. Thermal transient rough EHL line contact simulations by aid of computational fluid dynamics. Tribol Int 2008;41(8):683–93. http://dx.doi.org/10.1016/j.triboint.2007.11.004.
[15] Feldermann A, Neumann S, Jacobs G. CFD simulation of elastohydrodynamic lubrication problems with reduced order models for fluid–structure interaction. Tribol - Mater Surf Interfaces 2017;11(1):30–8. http://dx.doi.org/10.1080/17515831.2017.1279846.
[16] Paturi UMR, Palakurthy ST, Reddy NS. The role of machine learning in tribology: A systematic review. Arch Comput Methods Eng 2023;30(2):1345–97. http://dx.doi.org/10.1007/s11831-022-09841-5.
[17] Noé F, Tkatchenko A, Müller K-R, Clementi C. Machine learning for molecular simulation. Annu Rev Phys Chem 2020;71(1):361–90. http://dx.doi.org/10.1146/annurev-physchem-042018-052331.
[18] Ajuria Illarramendi E, Alguacil A, Bauerheim M, Misdariis A, Cuenot B, Benazera E. Towards an hybrid computational strategy based on deep learning for incompressible flows. In: AIAA AVIATIoN 2020 FORUM. AIAA AVIATIoN forum, American Institute of Aeronautics and Astronautics; 2020, p. 1–17. http://dx.doi.org/10.2514/6.2020-3058.
[19] Balasubramanian A, Guastoni L, Güemes A, Ianiro A, Discetti S, Schlatter P, Azizpour H, Vinuesa R. Predicting the near-wall region of turbulence through convolutional neural networks. 2021, arXiv preprint arXiv:2107.07340.
[20] Güemes A, Discetti S, Ianiro A, Sirmacek B, Azizpour H, Vinuesa R. From coarse wall measurements to turbulent velocity fields through deep learning. Phys Fluids 2021;33(7):075121. http://dx.doi.org/10.1063/5.0058346.

[21] Kochkov D, Smith JA, Alieva A, Wang Q, Brenner MP, Hoyer S. Machine learning–accelerated computational fluid dynamics. Proc Natl Acad Sci 2021;118(21):e2101784118. http://dx.doi.org/10.1073/pnas.2101784118.

[22] Hasan MS, Kordijazi A, Rohatgi PK, Nosonovsky M. Triboinformatic modeling of dry friction and wear of aluminum base alloys using machine learning algorithms. Tribol Int 2021;161:107065. http://dx.doi.org/10.1016/j.triboint.2021.107065.

[23] Wang Q, Wang X, Zhang X, Li S, Wang T. Tribological properties study and prediction of PTFE composites based on experiments and machine learning. Tribol Int 2023;188:108815. http://dx.doi.org/10.1016/j.triboint.2023.108815.

[24] Issa J, El Hajj A, Vergne P, Habchi W. Machine learning for film thickness prediction in elastohydrodynamic lubricated elliptical contacts. Lubricants 2023;11(12):497.

[25] Sinanoğlu C, Kurban AO, Yildirim S. Analysis of pressure variations on journal bearing system using artificial neural network. Ind Lubr Tribol 2004;56:74–87. http://dx.doi.org/10.1108/00368790410524038.

[26] Sinanoğlu C, Nair F, Karamiş MB. Effects of shaft surface texture on journal bearing pressure distribution. J Mater Process Technol 2005;168:344–53. http://dx.doi.org/10.1016/j.jmatprotec.2005.02.252.

[27] Fillon M, Bouyer J. Thermohydrodynamic analysis of a worn plain journal bearing. Tribol Int 2004;37(2):129–36. http://dx.doi.org/10.1016/S0301-679X(03)00051-3, Validation data.

[28] Ghorbanian J, Ahmadi M, Soltani R. Design predictive tool and optimization of journal bearing using neural network model and multi-objective genetic algorithm. Sci Iranica 2011;18(5):1095–105. http://dx.doi.org/10.1016/j.scient.2011.08.007.

[29] Hess N, Shang L. Machine learning prediction of journal bearing pressure distributions, considering elastic deformation and cavitation. In: ASME/bATH 2021 symposium on fluid power and motion control. Vol. ASME/BATH 2021 Symposium on Fluid Power and Motion Control, V001T01A010; 2021, http://dx.doi.org/10.1115/fpmc2021-68483.

[30] Rossopoulos GN, Papadopoulos CI. A journal bearing performance prediction method utilizing a machine learning technique. Proc Inst Mech Eng J: J Eng Tribol 2021;236(10):1993–2003. http://dx.doi.org/10.1177/13506501211055710.

[31] Kumar S, Kumar V, Singh AK. Deep neural network approach for the prediction of journal bearing static performance characteristics. In: Kumar R, Chauhan VS, Talha M, Pathak H, editors. Machines, mechanism and robotics. Springer Singapore; 2022, p. 1669–82. http://dx.doi.org/10.1007/978-981-16-0550-5_161.

[32] Baş H, Karabacak YE. Machine learning-based prediction of friction torque and friction coefficient in statically loaded radial journal bearings. Tribol Int 2023;186:108592. http://dx.doi.org/10.1016/j.triboint.2023.108592.

[33] Gheller E, Chatterton S, Panara D, Turini G, Pennacchi P. Artificial neural network for tilting pad journal bearing characterization. Tribol Int 2023;188:108833. http://dx.doi.org/10.1016/j.triboint.2023.108833.

[34] Marian M, Mursak J, Bartz M, Profito FJ, Rosenkranz A, Wartzack S. Predicting EHL film thickness parameters by machine learning approaches. Friction 2023;11(6):992–1013. http://dx.doi.org/10.1007/s40544-022-0641-6.

[35] Singh A, Wolf M, Jacobs G, König F. Machine learning based surrogate modelling for the prediction of maximum contact temperature in EHL line contacts. Tribol Int 2023;179:108166. http://dx.doi.org/10.1016/j.triboint.2022.108166.

[36] Elrod HG, Adams ML. A computer program for cavitation and starvation problems. Cavitation Relat Phenom Lubr 1974;37.

[37] Reynolds O. On the theory of lubrication and its application to mr. Beauchamp tower's experiments, including an experimental determination of the viscosity of olive oil. Philos Trans R Soc Lond 1886;177:157–234.

[38] Bouyer J, Fillon M. An experimental analysis of misalignment effects on hydrodynamic plain journal bearing performances. J Tribol 2001;124(2):313–9. http://dx.doi.org/10.1115/1.1402180.

[39] García S, Luengo J, Herrera F. Data preprocessing in data mining. Vol. 72, Springer; 2015.

[40] Lydia A, Francis S. Adagrad—an optimizer for stochastic gradient descent. Int J Inf Comput Sci 2019;6(5):566–8.

[41] Nvidia. CUDA zone - library of resources. 2023, URL https://developer.nvidia.com/cuda-zone.

[42] Vanhoucke V, Senior A, Mao MZ. Improving the speed of neural networks on CPUs. 2011.

[43] He M, Allaire P, Cloud C, Nicholas J. A pressure dam bearing analysis with adiabatic thermal effects. Tribol Trans 2010;January-March 2004:70–6. http://dx.doi.org/10.1080/05698190490279001.